Homeostasis for fiber circuits - Numerical tests

Higor S. Monteiro

August 5, 2021

Contents

1 FFF circuit with two input nodes

The diagram of this circuit is shown at Fig. 1.

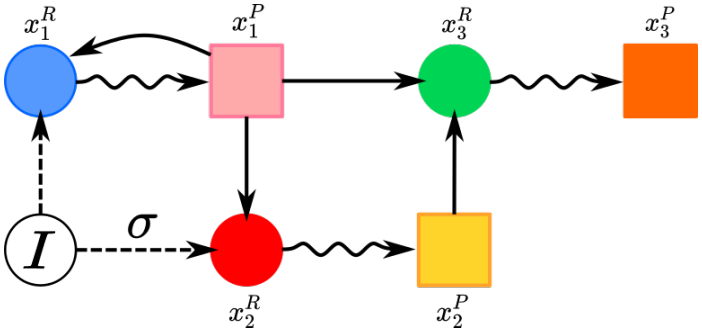

Figure 1: Feed-Forward Fiber circuit with two input nodes (x_1^R and x_2^R) and output node x_3^P.

The special model [3, 1] used for this circuit is given by the set of non-linear differential equations of Eq. 1:

$$\begin{aligned}
f_{x_1^R}(x_1^R, x_1^P, \mathcal{I}) &= -\delta x_1^R + \gamma \tilde{f}(x_1^P) + \mathcal{I} \\
f_{x_1^P}(x_1^P, x_1^R) &= -\alpha x_1^P + \beta x_1^R \\
f_{x_2^R}(x_2^R, x_1^P, \mathcal{I}) &= -\delta x_2^R + \gamma \tilde{f}(x_1^P) + \sigma\mathcal{I} \\
f_{x_2^P}(x_2^P, x_2^R) &= -\alpha x_2^P + \beta x_2^R \\
f_{x_3^R}(x_3^R, x_1^P, x_2^P) &= -\delta x_3^R + \gamma \tilde{g}(x_1^P, x_2^P) \\
f_{x_3^P}(x_3^P, x_3^R) &= -\alpha x_3^P + \beta x_3^R
\end{aligned}, \tag{1}$$

where $\tilde{f}$ and $\tilde{g}$ are monotonic nonlinear functions within the interval $[0, 1]$. Specifically, $\tilde{f}$ and $\tilde{g}$ are defined as Hill functions, and $\tilde{g}(x_1^P, x_2^P) = \tilde{g}(x_1^P + x_2^P)$.

The general infinitesimal homeostasis condition obtained by using the algorithm of [2], which is a generalization of [6] for multiple inputs, is given by Eq. 2 below:

$$\begin{aligned}
&+ f_{x_2^R,I} f_{x_2^P,x_2^R} f_{x_3^R,x_2^P} (f_{x_1^R,x_1^R} f_{x_1^P,x_1^P} - f_{x_1^R,x_1^P} f_{x_1^P,x_1^R}) \\
&+ f_{x_1^R,I} f_{x_1^P,x_1^R} (f_{x_2^R,x_1^P} f_{x_2^P,x_2^R} f_{x_3^R,x_2^P} + f_{x_2^R,x_2^R} f_{x_2^P,x_2^P} f_{x_3^R,x_1^P}) = 0'
\end{aligned} \tag{2}$$

which is translated to Eq. 3 according to Eq. 1 as:

$$\tilde{g}'(x_1^P + x_2^P)\Big\{\alpha\delta(1+\sigma) + \gamma\beta\tilde{f}'(x_1^P)(1-\sigma)\Big\} = 0. \tag{3}$$

From condition of Eq. 3, we can determine the relations to be satisfied together with the additional conditions for infinitesimal chair at some input value $\mathcal{I}_0$. Thus, we can state that a stable equilibrium $\vec{x}_\infty$ at $\mathcal{I}_0$ satisfies the infinitesimal homeostasis condition, $x^P_{3(\infty),\mathcal{I}}(\mathcal{I}_0) = 0$, iff

$$\rho(\mathcal{I}_0) \equiv \tilde{g}'(x_1^P + x_2^P)\Big\{\alpha\delta(1+\sigma) + \gamma\beta\tilde{f}'(x_1^P)(1-\sigma)\Big\} = 0, \tag{4}$$

and an infinitesimal chair point occurs if, according to the same assumptions, we satisfy the additional conditions

$$\frac{d\rho}{d\mathcal{I}}(\mathcal{I}_0) = 0 \quad \text{and} \quad \frac{d^2\rho}{d\mathcal{I}^2}(\mathcal{I}_0) \neq 0. \tag{5}$$

Following each one of the four conditions described above (equilibrium, infinitesimal homeostasis and the two conditions for infinitesimal chair), we can obtain the relations shown in Eq. 6 below:

$$\begin{aligned} \tilde{f}(x_1^P) &= \frac{\alpha\delta}{\beta\gamma}x_1^P - \frac{\mathcal{I}_0}{\gamma} \\ \tilde{f}'(x_1^P) &= -\frac{\alpha\delta}{\beta\gamma}\frac{(1+\sigma)}{(1-\sigma)}, \\ \tilde{f}''(x_1^P) &= 0 \\ \tilde{f}'''(x_1^P) &\neq 0 \end{aligned} \tag{6}$$

for $\sigma \neq 1$. Again, $\tilde{f}$ is either an increasing or decreasing monotonic nonlinear function within the interval $[0, 1]$ represented by a Hill function of exponent n. Note that from the second condition to the fourth, we assume that the homeostasis behavior is reached by considering that the second term of $\rho(\mathcal{I}_0)$ is zero. Thus, at first we ignore the possibility of $\tilde{g}'(x_1^P + x_2^P) = 0$, which happens only for total degradation ($x_1^P(\mathcal{I}) + x_2^P(\mathcal{I}) = 0$) or asymptotic saturation through $x_1^P(\mathcal{I}) + x_2^P(\mathcal{I}) \to \infty$, where ∞ only means that the sum is large enough to satisfy $\tilde{g}'(x_1^P + x_2^P) = 0$.

In order to perform numerical tests, we specify the form of $\tilde{f}$ and $\tilde{g}$ according to a Hill function $S(x)$(or $S(x+y)$ for $\tilde{g}$) of exponent $n = 2$. This way, we have

$$S(x) = \frac{1}{1+x^2} \quad \text{and} \quad S(x+y) = \frac{1}{1+(x+y)^2}, \tag{7}$$

from which we list the following derivatives:

$$\begin{aligned} S'(x) &= -\frac{2x}{(1+x^2)^2} \\ S''(x) &= -\frac{2(1-3x^2)}{(1+x^2)^3}. \\ S'''(x) &= \frac{24x(1-x^2)}{(1+x^2)^4} \end{aligned} \tag{8}$$

1.1 Case 1: $\tilde{f}(x) \equiv S(x)$ - UNSAT-FFF

By defining $\tilde{f} \equiv S(x)$, we consider that all regulations within the fiber (between nodes $x_1^R, x_1^P, x_2^R, x_2^P$) are repressors, which defines the UNSAT feed-forward fiber [4]. For this circuit the conditions defined in Eq. 6 is translated to conditions of Eq. 9:

$$\begin{aligned} S(x_1^P) &= \frac{\alpha\delta}{\beta\gamma}x_1^P - \frac{\mathcal{I}_0}{\gamma} \\ S'(x_1^P) &= -\frac{\alpha\delta}{\beta\gamma}\frac{(1+\sigma)}{(1-\sigma)}. \\ S''(x_1^P) &= 0 \\ S'''(x_1^P) &\neq 0 \end{aligned} \tag{9}$$

Now, from Eq. 9 and using the specific form of S and its derivatives displayed in Eq. 8, we perform further calculations to obtain the expression for $\mathcal{I}_0$.

From $S''(x_1^P) = 0$, we have that $x^P_{1(\infty)}(\mathcal{I}_0) = 1/\sqrt{3}$. $x^P_{1(\infty)}$ is the protein concentration 1 at the stable equilibrium $\vec{x}_\infty$. Then, from the equilibrium condition we obtain the expression for $\mathcal{I}_0$ in terms of the parameters of the special model:

$$\mathcal{I}_0 = \gamma\left(\frac{\alpha\delta}{\beta\gamma}\frac{1}{\sqrt{3}} - \frac{3}{4}\right), \tag{10}$$

which can be simplified by using the second condition and using $S'(x^P_{1(\infty)}) = -3\sqrt{3}/8$:

$$\frac{\alpha\delta}{\beta\gamma} = \frac{3\sqrt{3}}{8}\frac{(1-\sigma)}{(1+\sigma)}, \tag{11}$$

and finally we have the final form for the infinitesimal homeostasis point:

$$\mathcal{I}_0 = \gamma\left(\frac{3}{8}\frac{(1-\sigma)}{(1+\sigma)} - \frac{3}{4}\right). \tag{12}$$

Concerning $\tilde{g}(x_1^P + x_2^P)$, its specific form should influence only the set point defined by $x^P_{3(\infty)}$, but not at which value the homeostasis point $\mathcal{I}_0$ should occur (However, if x_1^P and x_2^P provides different regulations to x_3^P, we cannot represent $\tilde{g}(x_1^P, x_2^P)$ as $\tilde{g}(x_1^P + x_2^P)$ as showed in Eq. 7). We can also find relations for allowed values of σ considering the nonnegative model parameters and allowed values of $\mathcal{I}$, but for now we only make these relations explicit during the numerical tests (Fig. 2 and Fig. 3).

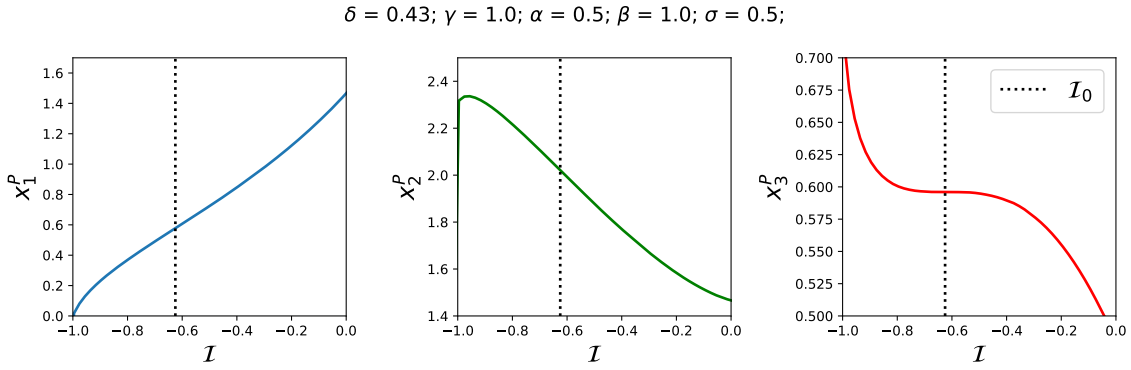

Figure 2: $\tilde{f}(x_1^P) \equiv S(x_1^P)$ and $\tilde{g}(x_1^P + x_2^P) \equiv S(x_1^P + x_2^P)$.

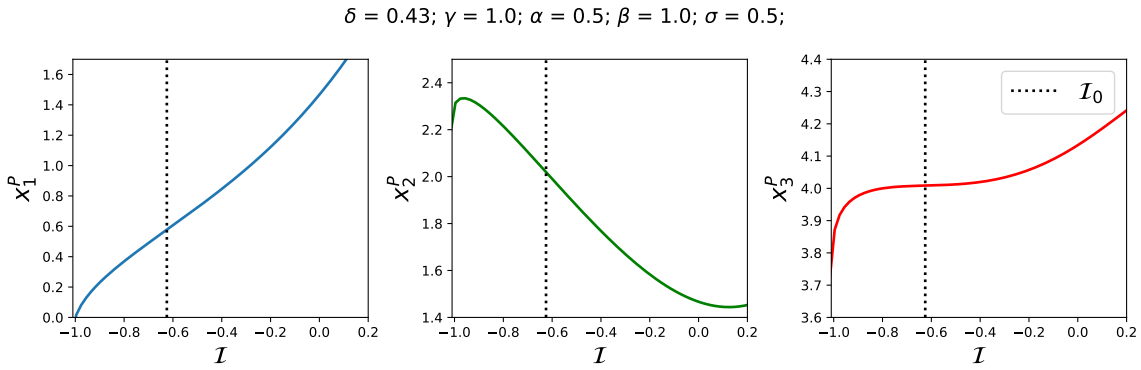

Figure 3: $\tilde{f}(x_1^P) \equiv S(x_1^P)$ and $\tilde{g}(x_1^P + x_2^P) \equiv 1 - S(x_1^P + x_2^P)$.

1.2 Case 2: $\tilde{f}(x) \equiv 1 - S(x)$ - SAT-FFF

By defining $\tilde{f} \equiv 1 - S(x)$, we consider that all regulations within the fiber (between nodes $x_1^R, x_1^P, x_2^R, x_2^P$) are activators, which defines the SAT feed-forward fiber [4]. For this circuit the conditions defined in Eq. 6 is trans-

lated to the relations of Eq. 13:

$$\begin{aligned} S(x_1^P) &= -\frac{\alpha\delta}{\beta\gamma}x_1^P + \left(1 + \frac{\mathcal{I}_0}{\gamma}\right) \\ S'(x_1^P) &= \frac{\alpha\delta}{\beta\gamma}\frac{(1+\sigma)}{(1-\sigma)} \\ S''(x_1^P) &= 0 \\ S'''(x_1^P) &\neq 0 \end{aligned} \quad . \tag{13}$$

Assuming that the second term of Eq. 3 is zero at $\mathcal{I}_0$, we can proceed with the calculations similarly as the UNSAT-FFF case before. Thus, following the conditions above, we obtain $x^P_{1(\infty)} = 1/\sqrt{3}$ for the stable equilibrium just as in the UNSAT-FFF case. From $S'(x^P_{1(\infty)})$, we obtain the relation

$$\frac{\alpha\delta}{\beta\gamma} = -\frac{3\sqrt{3}}{8}\frac{(1-\sigma)}{(1+\sigma)}, \tag{14}$$

from which we obtain the expression for the infinitesimal homeostasis point

$$\mathcal{I}_0 = -\gamma\left(\frac{3}{8}\frac{(1-\sigma)}{(1+\sigma)} + \frac{1}{4}\right). \tag{15}$$

Therefore, these conditions should be satisfied if $\rho(\mathcal{I}_0) = 0$ through its second term, meaning that $\tilde{g}'(x_1^P(\mathcal{I}) + x_2^P(\mathcal{I})) \neq 0$.

However, from what it is observed from the numerical calculations, these conditions are not fulfilled for positive regulations. We now show some of the numerical results obtained for the SAT-FFF and after we explain how the homeostasis is obtained for this circuit.

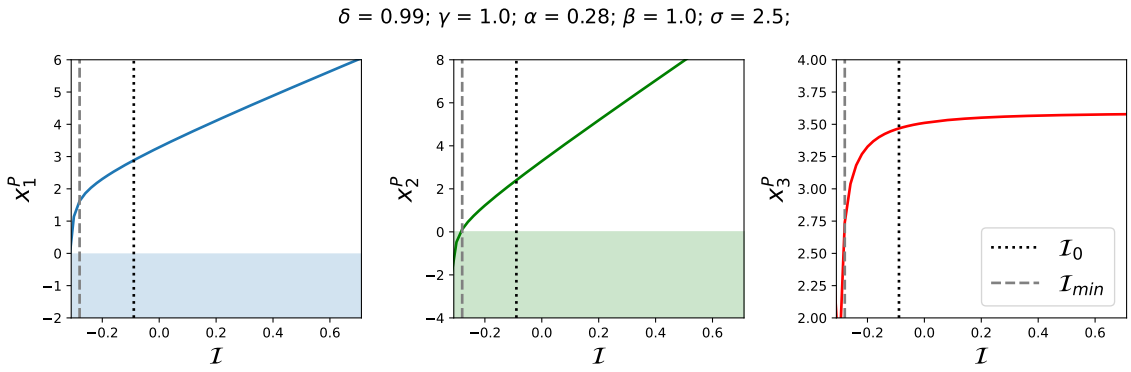

Figure 4: $\tilde{f}(x_1^P) \equiv 1 - S(x_1^P)$ and $\tilde{g}(x_1^P + x_2^P) \equiv 1 - S(x_1^P + x_2^P)$. $\mathcal{I}_0$ is the infinitesimal homeostasis point estimated from the vanishing condition of the second term of Eq. 4. $\mathcal{I}_{min}$ is the minimum value of $\mathcal{I}$ such that all protein concentrations are positive.

Considering the case above, $\tilde{f}(x_1^P) \equiv 1 - S(x_1^P)$ and $\tilde{g}(x_1^P, x_2^P) \equiv 1 - S(x_1^P + x_2^P)$, the system reaches homeostatic behavior by satisfying the first term of the product defining $\rho(\mathcal{I})$, Eq. 4, for all $\mathcal{I} > \mathcal{I}_c$, which is given by the first derivative of $\tilde{g}(x_1^P, x_2^P)$. $\mathcal{I}_c$ is some value for which $\tilde{g}'(x_1^P(\mathcal{I}), x_2^P(\mathcal{I})) \to 0$ for $\mathcal{I} > \mathcal{I}_c$. Moreover, all the derivatives of ρ also go to zero as all their terms contain high-order derivatives of $\tilde{g}(x_1^P, x_2^P)$ (in this case, a Hill function of the sum of the protein concentrations x_1^P and x_2^P):

$$\pm S^{(n)}(x_1^P(\mathcal{I}) + x_2^P(\mathcal{I})) \to 0 \Rightarrow \frac{d^{(n-1)}\rho}{d\mathcal{I}^{(n-1)}}(\mathcal{I}) \to 0 \quad \forall \mathcal{I} > \mathcal{I}_c. \tag{16}$$

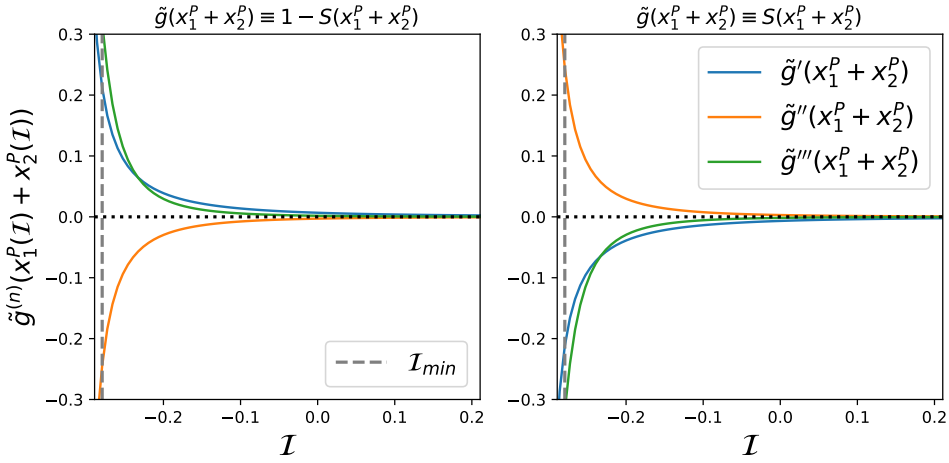

Figure 5: Higher-order derivatives of $\tilde{g}(x_1^P + x_2^P)$ as functions of the input parameter $\mathcal{I}$.

2 φ_2 Fibonacci circuit

In this section, we consider two possible input-output networks for the Fibonacci circuit ϕ_2 by changing the input node.

2.1 Input node x_1^R

The diagram of this circuit is shown at Fig. 6.

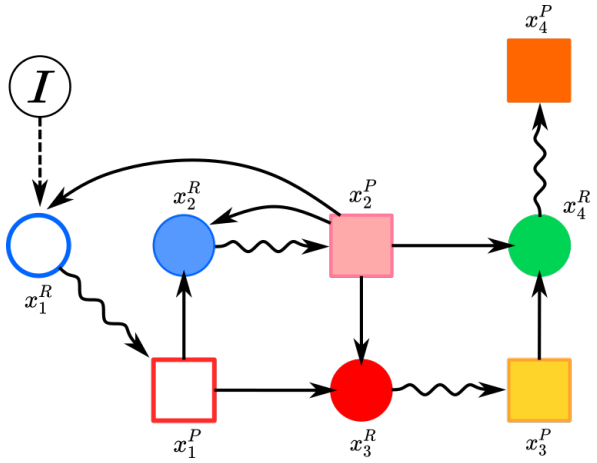

Figure 6: Fibonacci circuit φ_2 with input node x_1^R and output node x_4^P.

The special model [3, 1] used for this circuit is given by the set of non-linear differential equations of Eq. 17:

$$\begin{aligned}
f_{x_1^R}(x_1^R, x_2^P, \mathcal{I}) &= -\delta x_1^R + \gamma \tilde{f}(x_2^P) + \mathcal{I} \\
f_{x_1^P}(x_1^P, x_1^R) &= -\alpha x_1^P + \beta x_1^R \\
f_{x_2^R}(x_2^R, x_1^P, x_2^P) &= -\delta x_2^R + \gamma \tilde{g}(x_1^P, x_2^P) \\
f_{x_2^P}(x_2^P, x_2^R) &= -\alpha x_2^P + \beta x_2^R \\
f_{x_3^R}(x_3^R, x_1^P, x_2^P) &= -\delta x_3^R + \gamma \tilde{g}(x_1^P, x_2^P)' \\
f_{x_3^P}(x_3^P, x_3^R) &= -\alpha x_3^P + \beta x_3^R \\
f_{x_4^R}(x_4^R, x_2^P, x_3^P) &= -\delta x_4^R + \gamma \tilde{h}(x_2^P, x_3^P) \\
f_{x_4^P}(x_4^P, x_4^R) &= -\alpha x_4^P + \beta x_4^R
\end{aligned} \tag{17}$$

where $\tilde{f}$, $\tilde{g}$ and $\tilde{h}$ are monotonic nonlinear functions within the interval $[0, 1]$. Specifically, $\tilde{f}$, $\tilde{g}$ and $\tilde{h}$ are defined as Hill functions, with $\tilde{g}(x_1^P, x_2^P) = \tilde{g}(x_1^P + x_2^P)$ and $\tilde{h}(x_2^P, x_3^P) = \tilde{h}(x_2^P + x_3^P)$. For this circuit, we are imposing the restriction that the input function of x_2^R and x_3^R are given by the same function $\tilde{g}(x_1^P, x_2^P)$ which is motivated by the Fibonacci circuit realization in *E. Coli* gene network where all regulations within the fiber are repressors [5].

Using the algorithm of [6], we obtain the general infinitesimal homeostasis condition at point $\mathcal{I}_0$ for this input-output network according to the special model of Eq. 17:

$$2\alpha\delta\gamma^2\beta\tilde{g}'(x_1^P + x_2^P)\tilde{h}'(x_2^P + x_3^P) = 0. \tag{18}$$

Considering the condition of Eq. 18, we can determine the relations to be satisfied together with the additional conditions for infinitesimal chair

at $\mathcal{I}_0$. However, because of the simple form of Eq. 18, we only state the condition of infinitesimal homeostasis, $x^P_{4(\infty),\mathcal{I}}(\mathcal{I}_0) = 0$, for a given stable equilibrium $\vec{x}_\infty$ at $\mathcal{I}_0$, as

$$\rho(\mathcal{I}_0) \equiv \tilde{g}(x^P_1, x^P_2)\tilde{h}(x^P_2, x^P_3) = \tilde{g}(x^P_1 + x^P_2)\tilde{h}(x^P_2 + x^P_3) = 0, \tag{19}$$

which can only be satisfied for two cases: total degradation of the protein concentration ($x^P_{1,2}(\mathcal{I}) + x^P_{2,3}(\mathcal{I}) = 0$), or saturation of these same quantities: $x^P_{1,2}(\mathcal{I}) + x^P_{2,3}(\mathcal{I}) \to \infty$, where ∞ only means that the sum is large enough to satisfy either $\tilde{g}' = 0$ or $\tilde{h}' = 0$. Furthermore, by considering only these two possibilities we have that all the other higher-order derivatives also approach zero for those cases. We can observe the specifics of this type of behavior in the numerical example of Fig. 7.

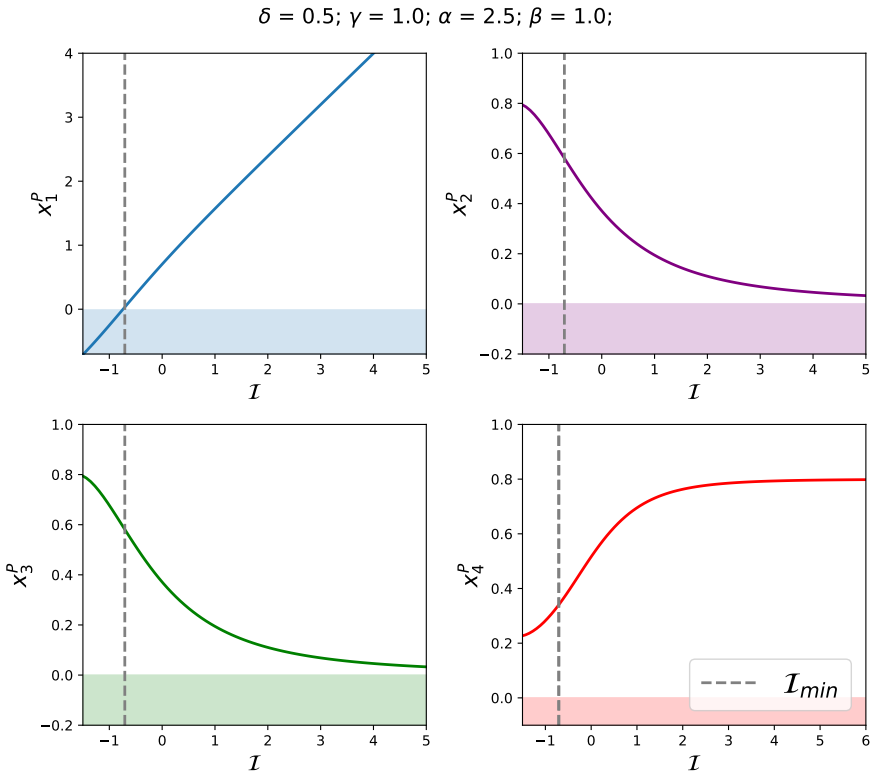

Figure 7: Protein concentrations for the Fibonacci circuit with input node x^R_1. By adding the input to x^R_1, the fibration symmetry is preserved and the concentrations of x^P_2 and x^P_3 are synchronized.

2.2 Input node x^R_2

The diagram of this circuit is shown at Fig. 8.

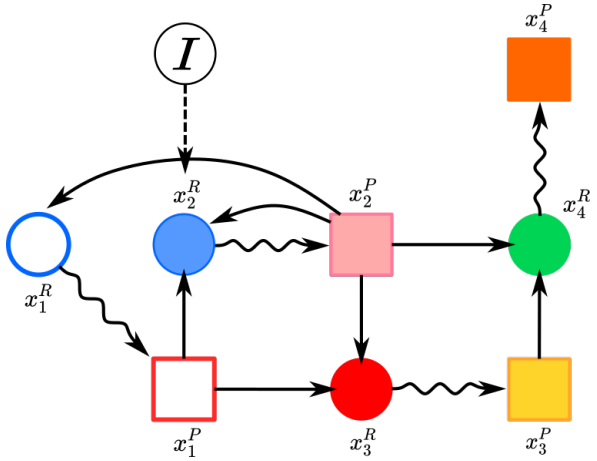

Figure 8: Fibonacci circuit φ_2 with input node x_2^R and output node x_4^P.

The special model [3, 1] used for this circuit is given by the set of non-linear differential equations of Eq. 20:

$$\begin{aligned}
f_{x_1^R}(x_1^R, x_2^P) &= -\delta x_1^R + \gamma \tilde{f}(x_2^P) \\
f_{x_1^P}(x_1^P, x_1^R) &= -\alpha x_1^P + \beta x_1^R \\
f_{x_2^R}(x_2^R, x_1^P, x_2^P, \mathcal{I}) &= -\delta x_2^R + \gamma \tilde{g}(x_1^P, x_2^P) + \mathcal{I} \\
f_{x_2^P}(x_2^P, x_2^R) &= -\alpha x_2^P + \beta x_2^R \\
f_{x_3^R}(x_3^R, x_1^P, x_2^P) &= -\delta x_3^R + \gamma \tilde{g}(x_1^P, x_2^P) \\
f_{x_3^P}(x_3^P, x_3^R) &= -\alpha x_3^P + \beta x_3^R \\
f_{x_4^R}(x_4^R, x_2^P, x_3^P) &= -\delta x_4^R + \gamma \tilde{h}(x_2^P, x_3^P) \\
f_{x_4^P}(x_4^P, x_4^R) &= -\alpha x_4^P + \beta x_4^R
\end{aligned} \tag{20}$$

where $\tilde{f}$, $\tilde{g}$ and $\tilde{h}$ are monotonic nonlinear functions within the interval $[0, 1]$. Specifically, $\tilde{f}$, $\tilde{g}$ and $\tilde{h}$ are defined as Hill functions, with $\tilde{g}(x_1^P, x_2^P) = \tilde{g}(x_1^P + x_2^P)$ and $\tilde{h}(x_2^P, x_3^P) = \tilde{h}(x_2^P + x_3^P)$. Following the same motivation of the previous circuit in subsection 2.1, we impose that the input function of x_2^R and x_3^R are given by the same function $\tilde{g}(x_1^P, x_2^P)$, according to what is observed in the gene network of *E. Coli* [5].

Using the algorithm of [6], we obtain the infinitesimal homeostasis condition at $\mathcal{I}_0$ for this particular input-output network according to the special model in Eq. 20. Therefore, we can state that at a given stable equilibrium $\bar{x}_{(\infty)}$ the infinitesimal homeostasis condition, $x^P_{4(\infty),\mathcal{I}}(\mathcal{I}_0) = 0$, is satisfied iff:

$$\rho(\mathcal{I}_0) \equiv \tilde{h}'(x_2^P, x_3^P)\left[\delta^2\alpha^2 + \delta\alpha\beta\gamma\tilde{g}'(x_1^P, x_2^P) + \gamma^2\beta^2\tilde{f}'(x_2^P)\tilde{g}'(x_1^P, x_2^P)\right] = 0. \tag{21}$$

This condition implies the additional conditions

$$\frac{d\rho}{d\mathcal{I}}(\mathcal{I}_0) = 0 \quad \text{and} \quad \frac{d^2\rho}{d\mathcal{I}^2}(\mathcal{I}_0) \neq 0 \tag{22}$$

for the infinitesimal chair condition.

Therefore, to satisfy Eq. 21 we have two possibilities: either the first term or the second term is zero at $\mathcal{I}_0$. The first scenario occurs only for $x_2^P(\mathcal{I}) + x_3^P(\mathcal{I}) = 0$ and $x_2^P(\mathcal{I}) + x_3^P(\mathcal{I}) \to \infty$, where ∞ here only means that the sum is large enough to satisfy the condition. Although this scenario is possible (as observed in the SAT-FFF), we consider only the second scenario, since it might provide more nontrivial homeostatic mechanisms.

Thus, by considering the four general condition for an infinitesimal chair point (equilibrium, $\rho(\mathcal{I}_0) = 0$, $\rho_{\mathcal{I}}(\mathcal{I}_0) = 0$ and $\rho_{\mathcal{I}\mathcal{I}}(\mathcal{I}_0) \neq 0$), we obtain the following relations:

$$\tilde{g}(x_1^P + x_2^P) = \frac{\alpha\delta}{\beta\gamma} x_2^P - \frac{\mathcal{I}}{\gamma}, \tag{23}$$

from the equilibrium condition. For $\rho(\mathcal{I}_0) = 0$, we have

$$\tilde{g}'(x_1^P + x_2^P) = -\frac{\alpha^2\delta^2}{\alpha\delta\beta\gamma + \gamma^2\beta^2\tilde{f}'(x_2^P)}. \tag{24}$$

Moreover, for $\rho_{\mathcal{I}}(\mathcal{I}_0) = 0$ and $\rho_{\mathcal{I}\mathcal{I}}(\mathcal{I}_0) \neq 0$, we obtain

$$\begin{aligned} &g''(x_1^P + x_2^P)(x_{1,\mathcal{I}}^P + x_{2,\mathcal{I}}^P)\Big[\alpha\delta\beta\gamma + \gamma^2\beta^2\tilde{f}'(x_2^P)\Big], \\ &+ \gamma^2\beta^2\tilde{g}'(x_1^P + x_2^P)\tilde{f}''(x_2^P)x_{2,\mathcal{I}}^P = 0 \end{aligned} \tag{25}$$

and

$$\begin{aligned} \Big\{\tilde{g}'''(x_1^P + x_2^P)(x_{1,\mathcal{I}}^P + x_{2,\mathcal{I}}^P)^2\Big[\alpha\delta\beta\gamma + \gamma^2\beta^2\tilde{f}'(x_2^P)\Big] \\ + \gamma^2\beta^2\tilde{f}'''(x_2^P)\tilde{g}'(x_1^P + x_2^P)(x_{2,\mathcal{I}}^P)^2\Big\} \neq 0 \end{aligned}, \tag{26}$$

respectively.

2.2.1 Key quantities

To perform the next calculations we assume that $\tilde{g}''(x_1^P + x_2^P) = 0$ and $\tilde{f}''(x_2^P) = 0$, such that Eq. 25 for $\rho_{\mathcal{I}}(\mathcal{I}_0)$ is satisfied. Therefore, we work on four cases regarding the combinations of the regulations $\tilde{f}$ and $\tilde{g}$. Before introducing these specific cases, let us calculate the main quantities to be used later.

Whether $\tilde{f} \equiv S$ or $\tilde{f} \equiv 1 - S$, we obtain $x^P_{2(\infty)} = \pm 1/\sqrt{3}$ for the protein concentration x^P_2 at equilibrium satisfying the partial chair condition $\tilde{f}''(x^P_2) = 0$, while from $\tilde{g}''(x^P_1 + x^P_2) = 0$ we have either $x^P_{1(\infty)} = 0$ or $x^P_{1,(\infty)} = \mp 2/\sqrt{3}$ for protein concentration x^P_1. This way, we have the following combinations for the concentrations x^P_1 and x^P_2 at homeostasis point:

$$\begin{aligned} x^P_{1,(\infty)} = 0 \ \text{ and } \ x^P_{2,(\infty)} = \pm\frac{1}{\sqrt{3}} \\ x^P_{1,(\infty)} = \mp\frac{2}{\sqrt{3}} \ \text{ and } \ x^P_{2,(\infty)} = \pm\frac{1}{\sqrt{3}} \end{aligned}, \tag{27}$$

giving a total four combinations for the concentrations x^P_1 and x^P_2 at the homeostasis point. We note that from these four combinations, only one provides a realistic scenario, since it does not predict negative concentrations either for x^P_1 or x^P_2.

Moreover, we calculate key quantities useful for the analysis of specific cases. First, regarding the first derivatives of $\tilde{f}$:

$$\begin{aligned} \tilde{f}'\Big(x^P_{2,(\infty)} = \pm\frac{1}{\sqrt{3}}\Big) = \mp\frac{3\sqrt{3}}{8} \ \ (\tilde{f} \equiv S) \\ \tilde{f}'\Big(x^P_{2,(\infty)} = \pm\frac{1}{\sqrt{3}}\Big) = \pm\frac{3\sqrt{3}}{8} \ \ (\tilde{f} \equiv 1 - S) \end{aligned}. \tag{28}$$

Now for $\tilde{g}$ and its first derivative. For $\tilde{g} \equiv S$, we have:

$$\begin{aligned} &\tilde{g}(x^P_{1,(\infty)} + x^P_{2,(\infty)}) = \frac{3}{4} \\ &\tilde{g}'\Big(x^P_{1,(\infty)} = 0, x^P_{2,(\infty)} = \pm\frac{1}{\sqrt{3}}\Big) = \mp\frac{3\sqrt{3}}{8} \\ &\tilde{g}'\Big(x^P_{1,(\infty)} = \mp\frac{2}{\sqrt{3}}, x^P_{2,(\infty)} = \pm\frac{1}{\sqrt{3}}\Big) = \pm\frac{3\sqrt{3}}{8} \\ &\mathcal{I}_0 = \gamma\Big[\frac{\alpha\delta}{\beta\gamma}x^P_{2,(\infty)} - \frac{3}{4}\Big], \quad \text{for} \quad x^P_{2,(\infty)} = \pm\frac{1}{\sqrt{3}} \end{aligned}, \tag{29}$$

and for $\tilde{g} \equiv 1 - S$:

$$\begin{aligned}
&\tilde{g}(x^P_{1,(\infty)} + x^P_{2,(\infty)}) = \frac{1}{4} \\
&\tilde{g}'(x^P_{1(\infty)} = 0,\ x^P_{2(\infty)} = \pm 1/\sqrt{3}) = \pm\frac{3\sqrt{3}}{8} \\
&\tilde{g}'(x^P_{1(\infty)} = \mp 2/\sqrt{3},\ x^P_{2(\infty)} = \pm 1/\sqrt{3}) = \mp\frac{3\sqrt{3}}{8} \\
&\mathcal{I}_0 = \gamma\left[\frac{\alpha\delta}{\beta\gamma}x^P_{2,(\infty)} - \frac{1}{4}\right], \quad \text{for} \quad x^P_{2,(\infty)} = \pm\frac{1}{\sqrt{3}}
\end{aligned} \tag{30}$$

2.2.2 Case 1: $\tilde{f}(x^P_2) \equiv S(x^P_2)$ and $\tilde{g}(x^P_1 + x^P_2) \equiv S(x^P_1 + x^P_2)$

Define $D = 3\sqrt{3}/8$. For $x^P_{1,(\infty)} = 0$ and $x^P_{2,(\infty)} = \pm 1/\sqrt{3}$ we obtain, from Eq. 25,

$$D^2\left(\frac{\gamma\beta}{\alpha\delta}\right)^2 \mp D\frac{\gamma\beta}{\alpha\delta} + 1 = 0, \tag{31}$$

which results only in complex values of $\gamma\beta/\alpha\delta$. This case is discarded for further analysis.

For $x^P_{1,(\infty)} = \mp 2/\sqrt{3}$ and $x^P_{2,(\infty)} = \pm 1/\sqrt{3}$ we obtain

$$-D^2\left(\frac{\gamma\beta}{\alpha\delta}\right)^2 \pm D\frac{\gamma\beta}{\alpha\delta} + 1 = 0, \tag{32}$$

which results in real values of $\gamma\beta/\alpha\delta$. More specifically, we have

$$\frac{\gamma\beta}{\alpha\delta} = \frac{4}{9}\left[\pm\sqrt{3} \mp^{root} \sqrt{15}\right], \tag{33}$$

where $\mp^{root}$ is independent of the signs of x^P_1 and x^P_2 at the equilibrium. Then, considering the Eq. 33 above, we have two main scenarios:

$$\frac{\gamma\beta}{\alpha\delta} = \frac{4}{9}\left[+\sqrt{3} \mp^{root} \sqrt{15}\right], \tag{34}$$

and

$$\frac{\gamma\beta}{\alpha\delta} = \frac{4}{9}\left[-\sqrt{3} \mp^{root} \sqrt{15}\right], \tag{35}$$

each one related to one combination between the values of $x^P_{1,(\infty)}$ and $x^P_{2,(\infty)}$. From the assumptions that all model parameters are nonnegative, we only consider the cases where $\mp^{root}$ leads to $\gamma\beta/\alpha\delta > 0$. Since here

both situations leads to one negative protein concentration, we only consider $x^P_{1,(\infty)} = +2/\sqrt{3}$ and $x^P_{2,(\infty)} = -1/\sqrt{3}$ to display the chair behavior around $\mathcal{I}_0$. Therefore, for $\gamma\beta/\alpha\delta > 0$, we have

$$\frac{\gamma\beta}{\alpha\delta} = \frac{4}{9}\Big[-\sqrt{3} + \sqrt{15}\Big], \tag{36}$$

and

$$\mathcal{I}_0 = -\gamma\left(\frac{\alpha\delta}{\beta\gamma}\frac{1}{\sqrt{3}} + \frac{3}{4}\right), \tag{37}$$

allowing us to obtain the chair behavior shown at Fig. 9.

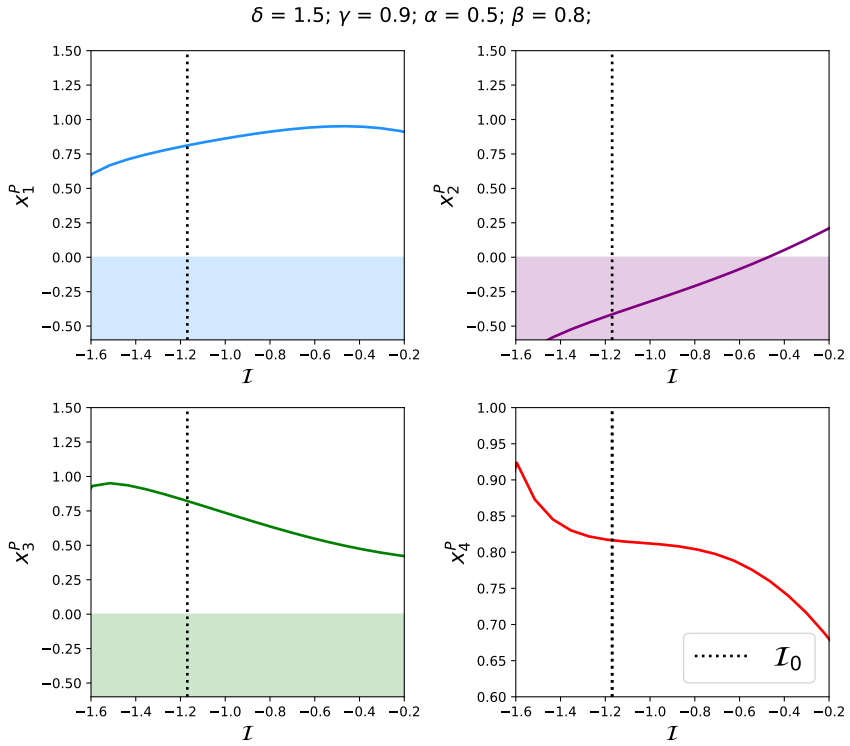

Figure 9: Protein concentrations for the Fibonacci circuit with input node x^R_2.

2.2.3 Case 2: $\tilde{f}(x^P_2) \equiv 1 - S(x^P_2)$ and $\tilde{g}(x^P_1 + x^P_2) \equiv S(x^P_1 + x^P_2)$

Define $D = 3\sqrt{3}/8$. For $x^P_{1,(\infty)} = \mp 2/\sqrt{3}$ and $x^P_{2,(\infty)} = \pm 1/\sqrt{3}$ we obtain, from Eq. 25,

$$D^2\left(\frac{\gamma\beta}{\alpha\delta}\right)^2 \pm D\frac{\gamma\beta}{\alpha\delta} + 1 = 0, \tag{38}$$

which results only in complex values of $\gamma\beta/\alpha\delta$. This case is discarded for further analysis.

For $x^P_{1,(\infty)} = 0$ and $x^P_{2,(\infty)} = \pm 1/\sqrt{3}$ we obtain

$$-D^2\left(\frac{\gamma\beta}{\alpha\delta}\right)^2 \mp D\frac{\gamma\beta}{\alpha\delta} + 1 = 0, \tag{39}$$

which results in real values of $\gamma\beta/\alpha\delta$. More specifically, we have

$$\frac{\gamma\beta}{\alpha\delta} = \frac{4}{9}\left[\mp\sqrt{3} \mp^{root} \sqrt{15}\right], \tag{40}$$

where $\mp^{root}$ is independent of the signs of x^P_1 and x^P_2 at the equilibrium. Then, considering the Eq. 40 above, we have two main scenarios:

$$\frac{\gamma\beta}{\alpha\delta} = \frac{4}{9}\left[-\sqrt{3} \mp^{root} \sqrt{15}\right], \tag{41}$$

and

$$\frac{\gamma\beta}{\alpha\delta} = \frac{4}{9}\left[+\sqrt{3} \mp^{root} \sqrt{15}\right], \tag{42}$$

each one related to one combination between the values of $x^P_{1,(\infty)}$ and $x^P_{2,(\infty)}$. Again, we only consider the cases where $\mp^{root}$ leads to $\gamma\beta/\alpha\delta > 0$. Here, there is one combination for which both concentrations $x^P_{1,(\infty)}$ and $x^P_{2,(\infty)}$ are nonnegative, and we consider this case to display the chair behavior around $\mathcal{I}_0$. Therefore, for $\gamma\beta/\alpha\delta > 0$, we have

$$\frac{\gamma\beta}{\alpha\delta} = \frac{4}{9}\left[-\sqrt{3} + \sqrt{15}\right], \tag{43}$$

and

$$\mathcal{I}_0 = \gamma\left(\frac{\alpha\delta}{\beta\gamma}\frac{1}{\sqrt{3}} - \frac{3}{4}\right), \tag{44}$$

allowing us to obtain the chair behavior shown at Fig. 10.

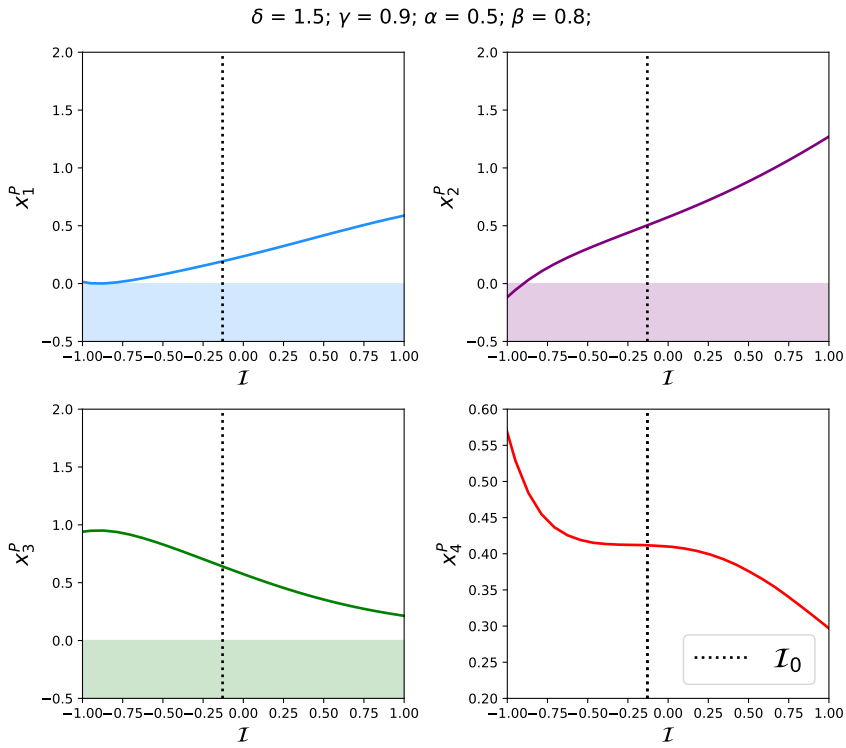

Figure 10: Protein concentrations for the Fibonacci circuit with input node x_2^R.

2.2.4 Case 3: $\tilde{f}(x_2^P) \equiv S(x_2^P)$ and $\tilde{g}(x_1^P + x_2^P) \equiv 1 - S(x_1^P + x_2^P)$

Define $D = 3\sqrt{3}/8$. For $x^P_{1,(\infty)} = \mp 2/\sqrt{3}$ and $x^P_{2,(\infty)} = \pm 1/\sqrt{3}$ we obtain, from Eq. 25,

$$D^2\left(\frac{\gamma\beta}{\alpha\delta}\right)^2 \mp D\frac{\gamma\beta}{\alpha\delta} + 1 = 0, \tag{45}$$

which results only in complex values of $\gamma\beta/\alpha\delta$. This case is discarded for further analysis.

For $x^P_{1,(\infty)} = 0$ and $x^P_{2,(\infty)} = \pm 1/\sqrt{3}$ we obtain

$$-D^2\left(\frac{\gamma\beta}{\alpha\delta}\right)^2 \pm D\frac{\gamma\beta}{\alpha\delta} + 1 = 0, \tag{46}$$

which results in real values of $\gamma\beta/\alpha\delta$. More specifically, we have

$$\frac{\gamma\beta}{\alpha\delta} = \frac{4}{9}\left[\pm\sqrt{3} \mp^{root} \sqrt{15}\right], \tag{47}$$

where $\mp^{root}$ is independent of the signs of x_1^P and x_2^P at the equilibrium. Then, considering the Eq. 47 above, we have two main scenarios:

$$\frac{\gamma\beta}{\alpha\delta} = \frac{4}{9}\left[+\sqrt{3} \mp^{root} \sqrt{15}\right], \tag{48}$$

and

$$\frac{\gamma\beta}{\alpha\delta} = \frac{4}{9}\Big[-\sqrt{3} \mp^{root} \sqrt{15}\Big], \tag{49}$$

each one related to one combination between the values of $x^P_{1,(\infty)}$ and $x^P_{2,(\infty)}$. Considering the cases where $\mp^{root}$ leads to $\gamma\beta/\alpha\delta > 0$, we have the combination for which both concentrations $x^P_{1,(\infty)} = 0$ and $x^P_{2,(\infty)} = +1/\sqrt{3}$ are nonnegative. We consider this case to display the homeostatic behavior around $\mathcal{I}_0$. Therefore, for $\gamma\beta/\alpha\delta > 0$, we have

$$\frac{\gamma\beta}{\alpha\delta} = \frac{4}{9}\Big[+\sqrt{3} + \sqrt{15}\Big], \tag{50}$$

and

$$\mathcal{I}_0 = \gamma\left(\frac{\alpha\delta}{\beta\gamma}\frac{1}{\sqrt{3}} - \frac{1}{4}\right), \tag{51}$$

which are the estimated values for the case where the second term of the product of Eq. 21 is zero. However, as we observe in Fig. 11 this condition is not fulfilled. Instead, the circuit reaches homeostasis by saturation through $\tilde{h}^{(n)}(x^P_2(\mathcal{I}) + x^P_3(\mathcal{I})) \to 0$ as $\mathcal{I} > \mathcal{I}_c$ for some real value $\mathcal{I}_c$ and integer n for high-order derivatives, as we can see in Fig. 12. Therefore, infinitesimal homeostasis $\rho(\mathcal{I}) = 0$ is satisfied by the vanishing of the first term of Eq. 21.

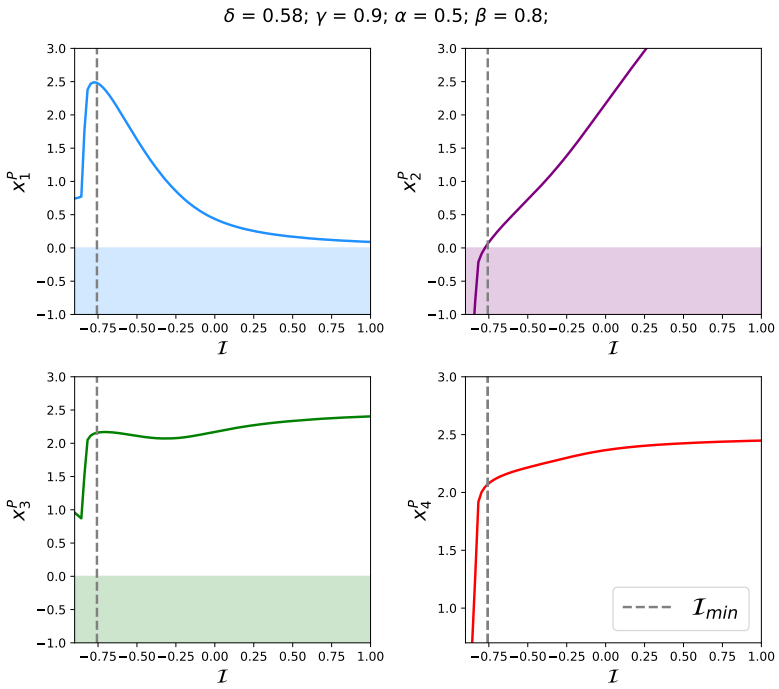

Figure 11: Protein concentrations for the Fibonacci circuit with input node x^R_2. $\mathcal{I}_{min}$ is the minimum value of $\mathcal{I}$ such that all protein concentrations are positive.

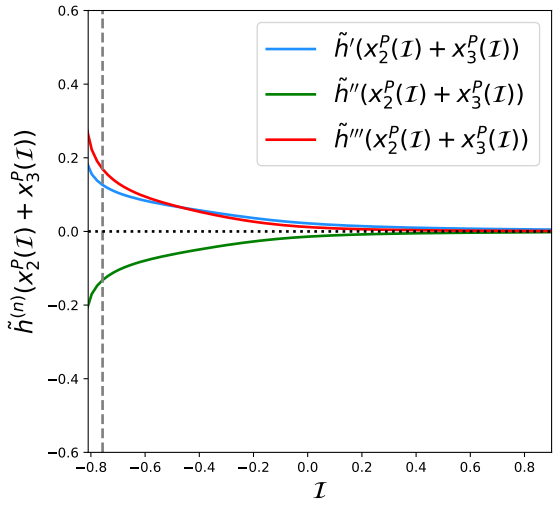

Figure 12: Higher-order derivatives of $\tilde{h}(x_2^P + x_3^P)$ as functions of the input parameter $\mathcal{I}$.

2.2.5 Case 4: $\tilde{f}(x_2^P) \equiv 1 - S(x_2^P)$ and $\tilde{g}(x_1^P + x_2^P) \equiv 1 - S(x_1^P + x_2^P)$

Define $D = 3\sqrt{3}/8$. For $x^P_{1,(\infty)} = 0$ and $x^P_{2,(\infty)} = \pm 1/\sqrt{3}$ we obtain, from Eq. 25,

$$D^2\left(\frac{\gamma\beta}{\alpha\delta}\right)^2 \pm D\frac{\gamma\beta}{\alpha\delta} + 1 = 0, \tag{52}$$

which results only in complex values of $\gamma\beta/\alpha\delta$. This case is discarded for further analysis.

For $x^P_{1,(\infty)} = \mp 2/\sqrt{3}$ and $x^P_{2,(\infty)} = \pm 1/\sqrt{3}$ we obtain

$$-D^2\left(\frac{\gamma\beta}{\alpha\delta}\right)^2 \mp D\frac{\gamma\beta}{\alpha\delta} + 1 = 0, \tag{53}$$

which results in real values of $\gamma\beta/\alpha\delta$. More specifically, we have

$$\frac{\gamma\beta}{\alpha\delta} = \frac{4}{9}\left[\mp\sqrt{3} \mp^{root} \sqrt{15}\right], \tag{54}$$

where $\mp^{root}$ is independent of the signs of x_1^P and x_2^P at the equilibrium. Then, considering the Eq. 54 above, we have two main scenarios:

$$\frac{\gamma\beta}{\alpha\delta} = \frac{4}{9}\left[-\sqrt{3} \mp^{root} \sqrt{15}\right], \tag{55}$$

and

$$\frac{\gamma\beta}{\alpha\delta} = \frac{4}{9}\left[+\sqrt{3} \mp^{root} \sqrt{15}\right], \tag{56}$$

each one related to one combination between the values of $x^P_{1,(\infty)}$ and $x^P_{2,(\infty)}$. Here we only consider the cases where $\gamma\beta/\alpha\delta > 0$. Also, since both situations satisfying $\gamma\beta/\alpha\delta > 0$ leads to one negative concentration we analyze the chair behavior only for the combination $x^P_{1,(\infty)} = +2/\sqrt{3}$ and $x^P_{2,(\infty)} = -1/\sqrt{3}$. Therefore,

$$\frac{\gamma\beta}{\alpha\delta} = \frac{4}{9}\Big[+\sqrt{3}+\sqrt{15}\Big], \tag{57}$$

and

$$\mathcal{I}_0 = -\gamma\left(\frac{\alpha\delta}{\beta\gamma}\frac{1}{\sqrt{3}}+\frac{1}{4}\right), \tag{58}$$

which are the estimated values for the case where the second term of the product of Eq. 21 is zero. Just like case 3, we observe in Fig. 13 that this condition is not fulfilled. Instead, the circuit reaches homeostasis again by saturation through $\tilde{h}^{(n)}(x^P_2(\mathcal{I}) + x^P_3(\mathcal{I})) \to 0$ as $\mathcal{I} > \mathcal{I}_c$ for some real value $\mathcal{I}_c$ and integer n for high-order derivatives, as we can see in Fig. 14. Therefore, infinitesimal homeostasis $\rho(\mathcal{I}) = 0$ is satisfied by the vanishing of the first term of Eq. 21. Furthermore, all the higher-order derivatives of $\tilde{h}$ also go to zero, satisfying all the higher derivatives $d^n\rho/d\mathcal{I}^n = 0$ and, thus, reaching a constant region for the input-output function $x^P_4(\mathcal{I})$.

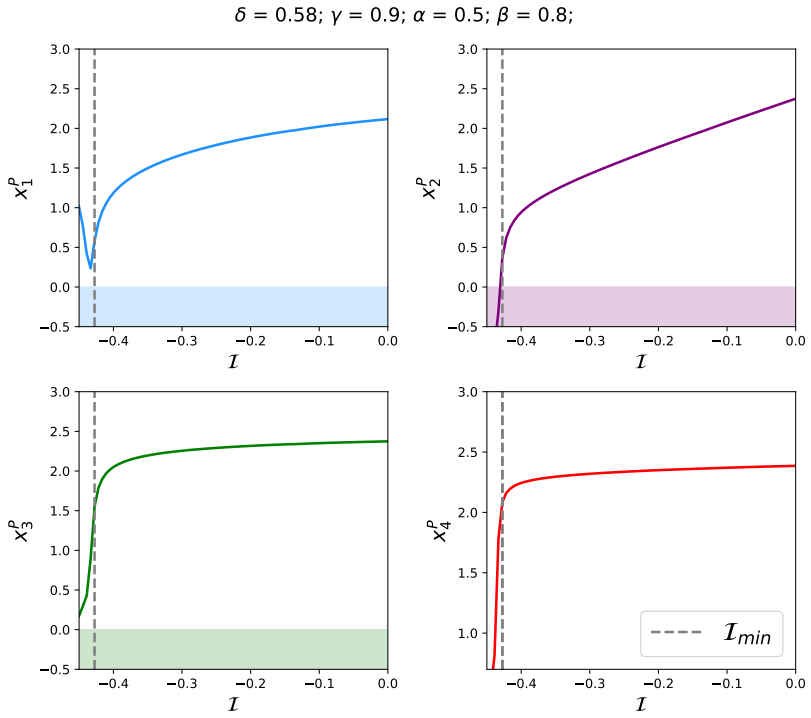

Figure 13: Protein concentrations for the Fibonacci circuit with input node x^R_2. $\mathcal{I}_{min}$ is the minimum value of $\mathcal{I}$ such that all protein concentrations are positive.

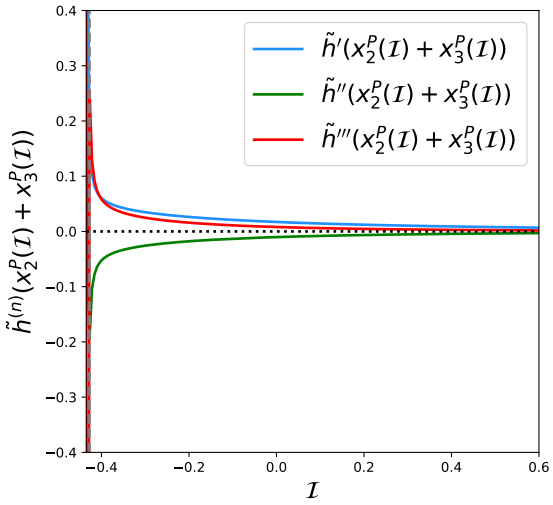

Figure 14: Higher-order derivatives of $\tilde{h}(x_2^P + x_3^P)$ as functions of the input parameter $\mathcal{I}$.

3 References

[1] Fernando Antonelli, Martin Golubitsky, and Ian Stewart. Homeostasis in a feed forward loop gene regulatory motif. *Journal of Theoretical Biology*, 445(103-109), 2018.

[2] João Luiz de Oliveira Madeira and Fernando Antoneli. Homeostasis in networks with multiple input nodes and robustness in bacterial chemotaxis, 2020.

[3] Mads Kærn, Timothy C. Elston, William J. Blake, and James J. Collins. Stochasticity in gene expression: from theories to phenotypes. *Nature Reviews Genetics*, 6:451–464, 2005.

[4] I. Leifer, F. Morone, S. D. S. Reis, J. S. Andrade, M. Sigman, and H. A. Makse. Circuits with broken symmetries perform core logic computations in genetic networks. *PLoS Comput. Biol.*, 16:1–16, 2020.

[5] Flaviano Morone, Ian Leifer, and Hernan A. Makse. Fibration symmetries uncover the building blocks of biological networks. *Proceedings of the National Academy of Sciences*, 117(15), 2020.

[6] Yangyang Wang, Zhengyuan Huang, Fernando Antoneli, and Martin Golubitsky. The structure of infinitesimal homeostasis in input–output networks. *Journal of Mathematical Biology*, 82(62), 2021.